Nuclear data - an essential tool in nuclear astrophysics

Karlheinz Langanke[1,2,*]

[1]GSI Helmholtzzentrum für Schwerionenforschung, Planckstr. 1, D-64291 Darmstadt, Germany
[2]Theoriezentrum, Institut für Kernphysik, Technische Universität Darmstadt, D-64291 Darmstadt, Germany

Abstract. Nuclear processes play an essential role for the evolution of many astrophysical objects and they are key to the origin of the elements in the Universe. Our understanding of the Universe has benefitted from the tremendous progress in nuclear physics which became possible due to novel experimental facilities and improved instrumentation as well as due to advances in theoretical modelling. The talk exemplifies this progress for three selected topics: solar and stellar hydrostatic burning, neutron-star mergers as a site of heavy-element production by the r-process and the influence of electron capture on nuclei for the core-collapse in massive stars leading to supernova explosions.

1 Introduction

Nuclear fusion reactions are the energy source during stellar hydrostatic burning which allow the stars' long lifetimes of millions to billions of years. Although during explosive stellar events, like supernovae or neutron-star mergers, the main energy reservoir is gravity, nuclear reactions, now involving shortlived nuclides, contribute decisively to the dynamics of the scenarios and the creation of elements in the Universe [1].

It is a challenge to determine the rate at which nuclear reactions occur in stellar environment. During hydrostatic burning, the stellar temperature is much smaller than the Coulomb barrier of the fusing nuclei. This makes it usually impossible to determine the cross sections at the most effective energies in stars in the laboratory. As a consequence, laboratory data measured at higher energies have to be extrapolated. Determining the properties of shortlived nuclides requires their artificial production in the laboratory which is possible for many, but not all nuclei at Radioactive Ion Beam (RIB) facilities and which has contributed to tremendous progress in astrophysical understanding in recent years. Furthermore, nuclear reaction rates are often modified in the stellar environment due to their high temperatures and densities. Such modifications require theoretical modelling, which has also advanced in recent years tremendously due to the increase of computational facilities and the development of novel theoretical approaches.

This manuscipt will highlight some of the recent experimental and theoretical progress focussing on nuclear data crucial for hydrostatic burning, the synthesis of heavy elements by the r-process and electron capture on nuclei as it is decisive for the core collapse of massive stars.

*e-mail: k.langanke@gsi.de

2 Hydrostatic burning

Recognizing the importance of nuclear fusion reactions, Fowler and his collaborators derived a series of tabulations in which they developed the formalism for an analytical presentation of stellar rates for easy use in stellar models. To facilitate the representation and to reduce the uncertainty in the extrapolation of data to lower energies, they defined the astrophysical S-factor $S(E)$ as the cross section with the known energy dependences (mainly the exponential energy dependence of Coulomb penetration) separated. In the absence of resonances, $S(E)$ is a function mildly varying with energy. By careful analysis of existing data and the extrapolation of $S(E)$, taking resonant contributions into account if appropriate, they recommended "best values" for the rates in a series of tabulations, [2, 3].

Modern rate tabulations are based on the same spirit, however, often extrapolating data in terms of energy dependences of the S-factor derived from nuclear models rather than simply assuming a McLaurin expansion as done in Fowler's original work. An example of paramount importance [4] is the $^{12}C(\alpha,\gamma)^{16}O$ reaction, which strongly influences the advanced evolution of stars and, together with the triple-α-reaction, determines the ratio of carbon and oxygen in the Universe. Here improved data, but also more reliable theoretical approaches have let to a strong reduction of the uncertainty of the rate at most effective energies during helium burning in Red Giants [5]. Another important reaction is the fusion of two ^{12}C nuclei. Here modern data and extrapolations, however, lead to somewhat conflicting results [6, 7]. Regularly updated tabulations of astrophysically relevant rates are provided by the Joint Institute of Nuclear Astrophysics on their webpages [8]

Arguably from all stars we know our Sun best. Solar models have drawn additional attention in recent decades due to the solar neutrino problem [9, 10] and its expla-

nation by neutrino oscillations [11]. Strong experimental efforts have decisively constrained the reaction rates of the pp-chains and the CNO cycle, where particular progress could be achieved by using dedicated underground laboratories to reduce disturbing backgrounds. A milestone has been the measurement of the ^{3}He+^{3}He cross section at solar energies directly at the LUNA facility in a tunnel underneath the Gran Sasso mountains in Italy [12]. Equivalently important has been the progress in few-body reaction theory and its applications to solar reactions. The continuing progress in experiment and theory for solar reactions has been extensively discussed in a series of publications in Reviews of Modern Physics [13, 14] (a new version is in preparation) and independently in Nuclear Physics [15]. It is impressive that the joint work of experimental and theoretical nuclear astrophysicists has transformed our Sun into a calibrated neutrino source.

It has been the traditional strategy to reduce the uncertainty of astrophysical reaction rates by measuring data to successively lower energies, hence decreasing the energy region for which the data have to be extrapolated. This strategy has faced a challenge as reactions of light particles have been measured at such low energies that they are influenced by the presence of electrons in the target (and the projectile) [16]. It has been argued that the adiabatic limit is applicable so that electron screening can be described by a constant increase of the relative energy of the fusion partners given by the difference in electron binding energy of the fused system and the separated projectile and target [16]. Hence electron screening would lead to an exponentially increasing enhancement of the measured cross sections compared to the bare nuclear case. Note that the bare nuclear cross section is needed for stellar modelling which is then modified due to plasma screening which is distinct from the laboratory case. The adiabatic approximation was confirmed in Time Dependent Hartree-Fock calculations [17]. However, experimental approaches yielded screening energies often noticeably larger than the adiabatic value [18–20]. This discrepancy requires a solution. A recent description of plasma and laboratory screening can be found in Ref. [21].

3 R-Process nucleosynthesis

The astrophysical r-process is a sequence of neutron captures and β-decays which produces about half of the elements heavier than iron [1]. It operates in environments with extreme neutron densities. By the observation of gravitational waves and the electromagnetic lightcurve (dubbed kilonova [22]) from the same event GW170817 [23, 24] it was demonstrated that neutron star mergers are one r-process site. Simulations of r-process nucleosynthesis in a neutron-star merger event (for example [25, 26]) shows that significant amount of matter is transported beyond the third r-process peak at mass number $A \sim 195$ in less than a second. During this period, matter is in $(n, \gamma) \Longleftrightarrow (\gamma, n)$ equilibrium supported by energies derived from nuclear β-decays. Nuclei with magic neutron number $N = 126$ serve as waiting points resulting in the formation of the third peak already during the equilibrium phase. The second r-process peak at $A \sim 130$, however, is not produced in this phase, but as the product of fission of the matter beyond the third peak after freeze-out from equilibrium.

As a characteristic, the r-process path in the nuclear chart runs through nuclei with such large neutron excess that most of them have yet not been produced in the laboratory and their properties have to be modelled. Due to the simulations (e.g. [25, 26]) these are masses, half-lives, cross sections for neutron capture and fission rates and yields. In the following we will discuss recent progress on these quantities.

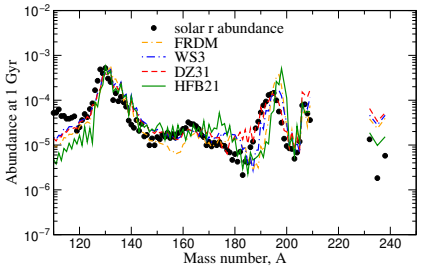

Figure 1. Dependence of r-process abundances on selected mass models. Figure taken from [26]. Reproduced with permission.

Traditionally global mass sets are based on the spirit of the liquid drop model, extended by microscopic insight derived from nuclear models. The parameters incorporated in these approaches are adjusted to known nuclear masses. Often used mass sets are the Finite Range Droplet Model (FRDM) [27], the Duflo-Zuker model (DZ31) [28] and an ansatz based on the Weizsäcker-Skyrme parametrization (WS3) [29]. As an alternative, global masses are also calculated within the microscopic HFB method (e.g. HFB21, [30]), where the effective interaction is adjusted to known masses. The global sets reproduce known data with an accuracy of about 100 keVs. The impact of masses on r-process abundances is shown in the Fig. 1. Noticeable differences can be seen in the reproduction of the third peak which are related to different predictions for the onset of deformation beyond the $N = 126$ magic number [26]. Also the amount of matter beyond the third peak depends on the masses. This has a significant effect on the power of the kilonova lightcurve which is decisively produced by α-decays of the heavy nuclei [22].

About 110 halflives of medium-mass nuclei at and close-to the r-process path have been recently measured at RIKEN [31]. This includes a few waiting-point nuclei in the second r-process peak. The half-lives of these nuclei with magic neutron number $N = 82$ agree well with large-scale shell model calculations [32, 33]. Shell-model calculations have also been performed for the $N = 126$ waiting points which govern the matter flow to heavier nuclei [32, 34]. These studies stress the importance of forbidden contributions to the half-lives, which are predicted noticeably shorter than anticipated before. A comparison to data is not possible as no r-process nucleus from the third peak has been produced yet. Unfortunately shell model studies for nuclei other than waiting points with magic neutron

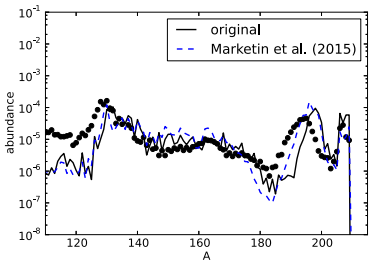

Figure 2. Dependence of r-process abundances on halflives (FRDM [35], HFB [37]). Figure taken from [38]. ©AAS. Reproduced with permission.

numbers are still prohibited due to computational restrictions. Thus global sets of r-process half-lives have been determined by QRPA calculations on the basis of phenomenological parametrizations [35] and of microscopic HFB or density functional approaches [36, 37, 39, 40], where the recent ones also include contributions from forbidden transitions. Fig. 2 shows the effect of half-lives on the r-process abundances where notiable differences are observed in the position of the third peak, but also for nuclei around mass number $A \sim 160$, which is a region of deformed nuclei.

Neutron capture rates become important for r-process simulations after it freezes out from equilibrium at temperatures below about 1 GK. Neutron capture rates are usually calculated within the statistical Hauser-Feshbach (HF) model [41]. An alternative approach is based on the direct capture potential model [42] which however has not sufficient predictive power if the stellar cross section is dominated by a single resonance [43]. Several of the ingredients in HF calculations have seen important advances in recent years. Nuclear level densities, including their parity- and angular momentum dependences, have been derived [45, 46] within the Shell Model Monte Carlo approach [44] exploiting its ability to derive thermally averaged nuclear properties in unprecedentedly large model spaces taking account of nuclear correlations by an effective interaction. Similar progress has been achieved based on a combination of HFB and combinatorial method [47]. These advances have been summarized in new global sets of level densities [48, 49] and are included in modern statistical model packages [50, 51]. A new experimental approach to determine level densities has been presented by the Oslo group based on measurements of gamma-strength functions [53].

Experimentally determined dipole γ-strength functions show an upbend of the strength towards low energies [52] which can have important effects on neutron capture rates [53, 54]. The upbend in the M1 strength has been studied and reproduced in shell model calculations for pf-shell and heavier nuclei [55].

A detailed and extensive review of the various aspects of r-process nucleosynthesis is given in Ref. [33], which also discusses advances in the description of fission rates and yields.

4 Electron captures on nuclei

A massive star ends its life in a supernova explosion triggered by the gravitational collapse of its inner core that is no longer supported by energy released in charged-particle reactions [56, 57]. During collapse, temperature is sufficiently large to bring reactions mediated by the strong and electromagnetic force into equilibrium with their inverses. Then the nuclear composition is given by Nuclear Statistical Equilibrium (NSE). Electrons form a relativistic degenerate electron gas and supply the pressure against the collapse.

The derivation of stellar electron capture rates is guided by two observations. First, within competing energy scales, the electron chemical potential μ_e grows much faster than the nuclear Q-values and temperature with growing density. Second, electron capture and the increase of density and temperature, drives the nuclear composition to more neutron-rich and heavy nuclei. These observations are the basis for a strategy by which stellar capture rates have been evaluated following the collapse from silicon burning to the formation of the homologuous core [58]. In the early collapse phase the nuclear Q-value and μ_e are comparable, both of the order a few MeV. At such low-energy conditions the capture is dominated by Gamow-Teller (GT) transitions. The composition is dominated by nuclei from the nickel-iron mass region (pf-shell nuclei). As $\mu_e \sim Q$, the capture rate is sensitive to the fragmentation of the GT distribution. For several relevant nuclei, the GT strength distribution has been measured by charge-exchange experiments (for reviews see [59, 60]). Importantly they are well reproduced by diagonalization shell model calculations [61, 62]. This is demonstrated in Fig. 3 which compares capture rates for pf-shell nuclei at early collapse conditions at which these nuclei are the most abundant. A detailed rate tabulation for individual pf-shell nuclei and at relevant astrophysical conditions is presented in [63]. Recently, shell model rates for Fe-Ni nuclei have been derived with an interaction which further improved the reproduction of the experimental GT strength [64]. In general, the modern shell model rates are noticeably smaller than those derived in the pioneering work by Fuller *et al.* [65] which were mainly based on the Independent Particle Model (IPM). The consequences of the shell model rates on silicon burning and the early collapse are discussed in [66, 67] and for thermonuclear supernovae in [68–70].

Electron captures are also essential for the final fate of intermediate mass stars with 8-12 $M_\odot$ which have developed an ONeMg core at the end of their hydrostatic burning [71]. With increasing density of core contraction, captures on ^{24}Mg and then on ^{20}Ne dominate the evolution. Both rates have been calculated with experimentally unknown GT transitions taken from the shell model [72, 73]. It turns out that the ^{20}Ne rate can be derived solely from experimental data [73] (Fig. 4). Importantly it is dominated at the most relevant astrophysical conditions by the second-forbidden transition between the ^{20}Ne and ^{20}F ground states, whose strength has recently been measured at Jyväskyla [74]. The impact of the new ^{20}Ne rate

on the core evolution of intermediate-mass stars is studied in [74–76].

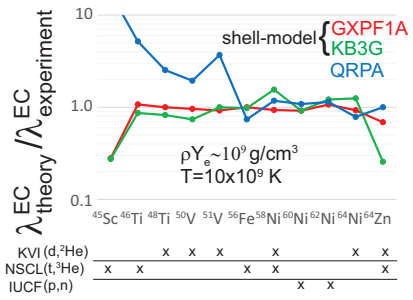

Figure 3. Comparison of electron captures rates, calculated from experimental GT data and distributions, derived from the large-scale shell model calculations with two different interactions (KB3G [62] and GXPF1 [64]) and from a Quasiparticle Random Phase Approximation (QRPA) approach [77]. The conditions correspond to the early stage of the collapse where the capture rates are sensitive to details of the GT distribution. The shell model rates have been quenched with the typical factor of $(0.74)^2$, as derived in [78]. ρY_e and T denote the electron density and temperature, respectively. KVI, UCSL and IUCF stay for the laboratories at which the experiments were performed. (Figure taken from [60])

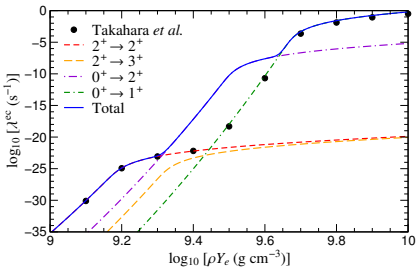

Figure 4. Electron capture rate for ^{20}Ne as function of density and for a specific temperature ($\log T[\mathrm{K}] = 8.6$) relevant for the core evolution of intermediate-mass stars. The rate is broken down to the individual state-by-state contributions. In the density regime, particularly relevant for core evolution, the rate is dominated by the second-forbidden ground-state-to-ground-state transition. The rates labeled 'Takahara et al.' are derived from allowed transitions calculated in the shell model [72]. (Figure taken from [73])

In the later stage of the collapse, the nuclei dominating the core composition become heavier and more neutron-rich, involving nuclei with proton numbers below $Z = 40$ and neutron numbers above $N = 40$. For such nuclei, the GT strength vanishes in the IPM due to Pauli blocking [79] which has led to the assumption in supernova simulations that electron capture is dominated by free protons rather than nuclei [56]. This is not true, as the GT strength is unblocked due to correlations across the $N = 40$ shell gap, as is experimentally proven for ^{76}Se [80], in good agreement with shell model calculations [81]. In general, the model space required for stellar electron capture calculations for nuclei with cross-shell correlations is too large to allow for shell model diagonalization calculations. However, this is also not needed as the electron chemical potential is now noticeably larger than the nuclear Q-value. Thus, rate calculations require most importantly a reliable description of cross-shell correlations [82] and a good reproduction of the total GT strength and its centroid. These requirements are fulfilled within a hybrid model [83–85] in which partial occupation numbers are calculated within the SMMC taking account of cross-shell correlations and these occupation numbers are then used in RPA calculation to determine the rates, also considering contributions from forbidden transitions which become increasingly importance with growing density.

At $N = 50$ the situation is different, as cross-shell correlations are too weak to unblock the GT strength, as experimentally demonstrated for ^{86}Kr and ^{88}Se, which show vanishing GT strength for the ground state [86, 87]. However, in the collapsing core $N = 50$ nuclei are only abundant at relatively high temperatures ($T \sim 1$ MeV). Then the situation is decisively different as thermal excitations mix orbitals across the shell gap and unblock the GT transitions. This was confirmed in two independent calculations for neutron-rich $N = 50$ nuclei using a thermal Quasiparticle Random Phase Approximation (QRPA) approach [88, 89], in agreement with the earlier results obtained within the SMMC studies [58, 84].

Based on the results of the diagonalization shell model for sd- and pf-shell nuclei and of the hybrid SMMC+RPA approach for heavier nuclei, electron capture rates have been tabulated for the full range of astrophysical conditions encountered during collapse of massive stars [58]. These rates, including appropriate screening corrections, are now incorporated in many of the leading supernova simulation codes. The impact on collapse simulations is significant [57, 84, 85]. Importantly capture on nuclei dominates over capture on free protons during the entire collapse.

A recent review of the experimental and theoretical progress to improve the derivation of stellar electron capture rates is given in Ref. [60]. The same progress also allowed for more reliable description of neutrino-nucleus cross sections and their role in supernovae, as reviewed in Ref. [90].

5 Outlook

Recent years have witnessed enormous progress in understanding the nuclear physics underlying many astrophysical objects. In this manuscript we have briefly summarized some of these advances which led to a better understanding of hydrostatic burning, in particular in our Sun, the synthesis of heavy elements by the astrophysical r-process and weak processes (here restricted to electron captures) involved in supernovae dynamics. This progress was made possible by improved computational facilities and nuclear models, but also due to the availability of new experimental facilities and instrumentation, in particular of Rare Isotope Laboratories like RIKEN. This trend will continue and accelerate, once the new RIB facilities FRIB and FAIR are fully in operation.

References

[1] E.M. Burbidge *et al.*, Rev. Mod. Phys. **29** 547 (1957).
[2] W.A. Fowler, G.R. Caughlan and B.A. Zimmerman, Ann. Rev. Astron. Astrophys. **5** 525 (1967)
[3] G.R. Cauglan and W. A Fowler, Nucl. Phys. **A40** 283 (1988)
[4] W.A. Fowler, Rev. Mod. Phys. **56** 149 (1984).
[5] R.J. deBoer *et al.*, Rev. Mod. Phys. **89** 035007 (2017)
[6] A. Tumino *et al.*, Nature **557** 687 (2018)
[7] W.P. Tan *et al.*, Phys. Rev. Lett. **124** 192702 (2020)
[8] https://reaclib.jinaweb.org
[9] R. Davies Jr., Rev. Mod. Phys. **75** 985 (2003)
[10] J.N. Bahcall, A.M. Serenelli and S. Basu, ApJ L85 621 (2005)
[11] A.B. McDonald, Rev. Mod. Phys. **88** 030502 (2016).
[12] R. Bonetti *et al.*, Phys. Rev. Lett. **82** 5205 (1999)
[13] E.G. Adelberger *et al.*, Rev. Mod. Phys. **70** 1265 (1998)
[14] E.G. Adelberger *et al.*, Rev. Mod. Phys. **83** 195 (2011)
[15] C. Angulo *et al.*, Nucl. Phys. **A656** 3 (1999)
[16] H.J. Assenbaum, K. Langanke and C.E. Rolfs, Z. Phys. **A327** 461 (1987)
[17] T.D. Shoppa *et al.*, Phys. Rev. **C48** 837 (1993)
[18] S. Engstler *et al.*, Phys. Lett. **B202** 179 (1988)
[19] S. Engstler *et al.*, Phys. Lett. **B279** 20 (1992)
[20] M. Aliotta *et al.*, Nucl. Phys. **A690** 790 (2001)
[21] M. Aliotta and K. Langanke, Frontiers in Physics **10** 942726 (2022)
[22] B.D. Metzger *et al.*, Mon. Not. R. Astron. Soc. **406** 2650 (2010).
[23] B.P. Abbott *et al.*, Astrophys. J. Lett. **848** L12 (2017).
[24] P.S. Cowperthwaite *et al.*, Astrophys. J. Lett. **848** L17 (2017).
[25] S. Goriely, A. Bauswein and H.-T. Janka, Astr. J. Lett. **738** L32 (2011).
[26] J.J. Mendoza-Temis *et al.* Phys. Rev. **92** 055805 (2015).
[27] P. Möller *et al.*, At. Data Nucl. Data Tables **59** 185 (1995)
[28] J. Duflo and A.P. Zuker, Phys. Rev. **C52** R23 (1995)
[29] N. Wang, M. Liu and X. Wu, Phys. Rev. **C81** 044322 (2010)
[30] S. Goriely, N. Chamel and J.M. Pearson, Phys. Rev. **C82** 3894 (2016)
[31] G. Lorusso *et al.* Phys. Rev. Lett. **114** 192501 (2015).
[32] Q. Zhi *et al.* Phys. Rev. **C87** 025803.
[33] J.J. Cowan *et al.* Rev. Mod. Phys. **93** 015002 (2021).
[34] T. Suzuki *et al.* Phys. Rev. **C85** 015802 (2012).
[35] P. Möller, J.R. Nix and K.-L. Kratz, At. Nucl. Data Tables **66** 131 (1997).
[36] I.N. Borzov, Phys. Rev. **C67** 025802 (2003).
[37] T. Marketin, L. Huther and G. Martínez-Pinedo, Phys. Rev. **C93** 025805 (2016).
[38] M. Eichler *et al.*, Astr. Astrophys. **808** 30 (2015).
[39] T. Shafer *et al.* Phys. Rev. **C94** 055802 (2016).
[40] E.M. Ney, J. Engel and N. Schunck, Phys. Rev. **C102** 034326 (2020).
[41] T. Rauscher, F.-K. Thielemann and K.L. Kratz, Phys. Rev. **C56** 1613 (1997)
[42] Y. Xu and S. Goriely, Phys. Rev. **C86** 045801 (2012)
[43] H.P. Loens *et al.* Eur. Phys. J **A48** 34 (2012)
[44] S.E. Koonin, D.J. Dean and K. Langanke, Phys. Rep. **278** 2 (1997).
[45] H. Nakada and Y. Alhassid, Phys. Rev. Lett. **79** 2939 (1997).
[46] Y. Alhassid, S. Liu and H. Nakada Phys. Rev. Lett. **99** 162504 (2007).
[47] S. Goriely, S. Hilaire and A.J. Koning, Phys. Rev. **C78** 064307 (2008).
[48] D. Mocelj *et al.*, Phys. Rev. **C75** 045805 (2007).
[49] S. Goriely, S. Hilaire and M. Girod, J. Phys. Conf. Ser. **337** 012027 (2012).
[50] A.J. Koning, S. Hilaire and S.Goriely, Nucl. Phys. **A810** 13 (2008.
[51] T. Rauscher, Int. J. Mod. Phys. **E20** 1071 (2011).
[52] M. Guttormsen *et al.*, Phys. Rev. **C71** 044307 (2005).
[53] A.C. Larsen *et al.*, Prog. Part. Nucl. Phys. **107** 69 (2019).
[54] S. Goriely, Phys. Lett. **B436** 10 (1998).
[55] K. Sieja, Phys. Rev. **C98** 064312 (2018).
[56] H.A. Bethe, Rev. Mod. Phys. **62** 801 (1990).
[57] H.-T. Janka *et al.* Phys. Rep. **442** 38 (2007).
[58] A. Juodagalvis *et al*, Nucl. Phys. **A848** 454 (2010).
[59] D. Frekers and M. Alanssari, Eur. Phys. J. **A54** 177 (2018).
[60] K. Langanke, G. Martinez-Pinedo, R.G.T. Zegers, Rep. Prog. Phys. **84** 066301 (2021)
[61] E. Caurier *et al.*, Nucl. Phys. **A653** 439 (1999).
[62] K. Langanke and G. Martínez-Pinedo, Nucl. Phys. **A673** 481 (2000).
[63] K. Langanke and G. Martínez-Pinedo, At. Data Nucl. Data Tables **79** 1 (2001).
[64] M. Honma *et al.*, Phys. Rev. **C69** 034335 (2004).
[65] G.M. Fuller, W.A. Fowler and M.J. Newman, Astr. J. Suppl. Ser. **48** 279 (1982).
[66] A. Heger *et al.*, Phys. Rev. Lett. **86** 1678 (2001).
[67] A. Heger *et al.*, Astrophys. J. **560** 307 (2001).
[68] F. Brachwitz *et al.* Astrophys. J. **536** 934 (2000).
[69] K. Langanke and G. Martinez-Pinedo, Rev. Mod. Phys. **75** 819 (2003)
[70] K. Mori *et al.*, Astr. J. **863** 176 (2018).
[71] K. Nomoto, Astr. J. **322** 206 (1987).
[72] M. Takahara, *et al.* Nucl. Phys. **A504** 167 (1989).
[73] G. Martínez-Pinedo, *et al.* Phys. Rev. **C89** 045806 (2014).
[74] O.S. Kirsebom *et al.*, Phys. Rev. Lett. **123** 262701 (2019).
[75] O.S. Kirsebom *et al.*, Phys. Rev. **C100** 065805 (2019).
[76] S. Zha *et al.*, Astr. J. **886** 22 (2019).
[77] A.L. Cole *et al.*, Phys. Rev. **C82** 015809 (2012).

[78] G. Martínez-Pinedo *et al.*, Phys. Rev. **C53** R2602 (1996).
[79] G.M. Fuller, Astr. J. **252** 741 (1982).
[80] E.W. Grewe *et al.*, Phys. Rev. **78** 044301 (2008).
[81] Q. Zhi *et al.*, Nucl. Phys. **A859** 172 (2011).
[82] D.J. Dean *et al.*, Phys. Rev. **C59** 2474 (1999).
[83] K. Langanke, E. Kolbe and D.J. Dean, Phys. Rev. **C63** 032801 (2001)
[84] K. Langanke *et al.*, Phys. Rev. Lett. **90** 241102 (2003).
[85] R.W. Hix *et al.*, Phys. Rev. Lett. **90** 210102 (2003).
[86] R. Titus *et al.*, Phys. Rev. **100** 045805 (2019).
[87] J.C. Zamora *et al.*, Phys. Rev. **100** 032801 (2019).
[88] A.A. Dzhioev *et al.*, Phys. Rev. **C101** 025805 (2020).
[89] E. Litvinova and C. Robin, Phys. Rev. **C103** 024326 (2021).
[90] K.G. Balasi, K. Langanke and G. Martinez-Pinedo, Prog. Nucl. Part Phys. **85** 1 (2015)